The Astrophysical Journal, 587:739–747, 2003 April 20

A TRIPLE RADIO CONTINUUM SOURCE ASSOCIATED WITH IRAS 16547–4247: A COLLIMATED STELLAR WIND EMANATING FROM A MASSIVE PROTOSTAR

Guido Garay
Departamento de Astronomía, Universidad de Chile, Casilla 36-D, Santiago, Chile

Kate J. Brooks
Departamento de Astronomía, Universidad de Chile, Casilla 36-D, Santiago, Chile;
and European Southern Observatory, Casilla 19001, Santiago 19, Chile

Diego Mardones
Departamento de Astronomía, Universidad de Chile, Casilla 36-D, Santiago, Chile

and

Ray P. Norris
Australia Telescope National Facility, P.O. Box 76, Epping, NSW 1710, Australia
Received 2002 November 19; accepted 2003 January 1

ABSTRACT

We report the discovery, made using the Australia Telescope Compact Array, of a triple radio source toward IRAS 16547−4247, a luminous infrared source with a bolometric luminosity of $6.2 \times 10^4\ L_\odot$. The radio source shows an almost linear structure consisting of a compact central object and two outer lobes separated by about 20″, located symmetrically to the central source. The radio emission from the lobes has spectral indices of −0.61 and −0.33, characteristic of nonthermal emission. The emission from the central object has a spectral index of 0.49, consistent with free-free emission from a thermal jet. Also reported are 1.2 mm continuum and molecular line observations made with the Swedish ESO Submillimeter Telescope. The 1.2 mm observations show that the dust emission arises from a region of 33″ × 25″ (FWHM) with a total flux of 16.4 Jy, implying a mass of $1.3 \times 10^3\ M_\odot$. The line observations indicate that IRAS 16547−4247 is associated with a molecular core with a FWHM deconvolved angular size of 27″ (diameter of 0.38 pc at the distance of 2.9 kpc), a molecular hydrogen density of 5.2×10^5 cm^{-3}, and a mass of $9.0 \times 10^2\ M_\odot$. We propose that this dense massive core hosts a high-mass star in an early stage of evolution in which it is undergoing the ejection of a collimated stellar wind. The radio emission from the lobes arises in shocks resulting from the interaction of this collimated wind with the surrounding medium. Our observations indicate that the jets found in the formation of low-mass stars are also produced in high-mass stars, with IRAS 16547−4247 being the most luminous young stellar object presently known to host a jet.

Subject headings: ISM: individual (IRAS 16547−4247) — ISM: jets and outflows — radio continuum: stars — stars: formation

1. INTRODUCTION

Massive stars ($M > 8\ M_\odot$) are known to form within dense and massive molecular cores (Churchwell, Walmsley, & Cesaroni 1990; Cesaroni et al. 1991; Plume, Jaffe, & Evans 1992). However, the sequence of processes leading to their formation is not yet well established. Our present understanding of star formation is based primarily on the observations of low-mass stars. In the current paradigm of the formation of low-mass stars (Shu, Adams, & Lizano 1987; Shu et al. 1993), there are four major evolutionary stages: (1) an initial stage in which the central region of a dense core begins to condense quasi-statically through the process of ambipolar diffusion; (2) an accretion stage, characterized by the presence of a central protostar and a circumstellar disk surrounded by an infalling envelope of dust and gas; (3) a phase in which the protostar deposits linear and angular momentum and mechanical energy into its surroundings through jets and molecular outflows; and finally, (4) a relatively more advanced phase in which the protostar settles onto the zero-age main sequence (ZAMS). Although this accretion paradigm has been very successful in explaining what is observationally known about the formation of low-mass stars (Lada 1991; Evans 1999), its applicability to the formation of massive stars remains arguable.

It is possible that massive stars are formed by processes that are radically different from those that produce low-mass stars. For instance, Bonnell, Bate, & Zinnecker (1998) have suggested that high-mass stars form by the merging of lower mass protostars. This coalescence scenario gains support by the fact that massive stars form in denser clusters than low-mass stars, where more dynamical interactions may take place. The role of coalescence (Stahler, Palla, & Ho 2000) and accretion (Osorio, Lizano, & D'Alessio 1999; McKee & Tan 2002) processes in the assembling of a massive star is still under debate. If massive O stars are formed by accretion, we expect that disks and jets will be generated in their earliest stages of evolution. On the other hand, if they are formed through coalescence of lower mass stars, then neither disks nor jets are expected. The search for jets and disks toward massive young stellar objects (YSOs) is thus crucial to understanding their formation process.

The recognition that outflows are produced by stars of all masses was established early on with the detection of powerful molecular outflows toward a few high-mass star-forming regions (Kwan & Scoville 1976; Rodríguez, Ho, & Moran 1980; Bally & Lada 1983; Lada 1985). More recently, systematic surveys have shown that molecular outflows are also a common phenomenon toward high-mass protostellar objects (Zhang et al. 2001; Beuther et al. 2002). The data

gathered in these studies show that there is a strong correlation between the molecular mass outflow rate and the luminosity of the driving source (Shepherd & Churchwell 1996; Churchwell 2000), suggesting that there is a strong link between accretion and outflow for a wide range of luminosities. This might also argue for a similar mechanism of formation for stars of all masses. However, more compelling evidence will be provided by the detection of disks and jets toward high-mass protostars.

Only a few massive YSOs are known to be associated with highly collimated jets and/or Herbig-Haro (HH) objects, all of which have luminosities smaller than $2 \times 10^4\ L_\odot$. They include IRAS 18162−2048 ($L \sim 1.7 \times 10^4\ L_\odot$; Martí, Rodríguez, & Reipurth 1993), Cepheus A HW2 ($L \sim 1 \times 10^4\ L_\odot$; Rodríguez et al. 1994), IRAS 20126+4104 ($L \sim 1.3 \times 10^4\ L_\odot$; Cesaroni et al. 1997), G192.16−3.82 ($L \sim 3 \times 10^3\ L_\odot$; Shepherd et al. 1998; Devine et al. 1999; Shepherd, Claussen, & Kurtz 2001), and W75N, which contains several molecular and HH outflows powered by at least four late- to early-B protostars (Shepherd, Testi, & Stark 2003). There is, however, a lack of observed young massive stars with spectral types earlier than B0 ZAMS, or $L > 2 \times 10^4\ L_\odot$, associated with jets and/or disks. Whether this is an intrinsic property of the most massive stars or due to an observational disadvantage—massive stars are rarer and their evolutionary timescales are much shorter than those of low-mass stars—has yet to be discerned.

In this paper, we present the discovery, made using the Australia Telescope Compact Array (ATCA),[1] of a triple radio continuum source powered by a young massive star associated with IRAS 16547−4247. Located at the distance of 2.9 kpc, this source has a luminosity of $6.2 \times 10^4\ L_\odot$. The source was selected from the catalog of *IRAS* sources with colors of compact H II regions and CS($2 \rightarrow 1$) emission reported by Bronfman, Nyman, & May (1996). The CS($2 \rightarrow 1$) spectra showed a self-absorbed profile with a strong blueshifted peak, consistent with inward motions (Mardones 1998) and extended line wings, indicating the presence of a molecular outflow. These characteristics and the high luminosity indicated that IRAS 16547−4247 corresponds to a young massive star-forming region. In the present study, we propose that the triple radio source detected toward IRAS 16547−4247 indicates the presence of a central highly collimated stellar wind source and two outer lobes of shock-ionized gas resulting from the interaction of the collimated wind with the surrounding medium. Objects with similar morphologies have been previously found to be associated with low-luminosity YSOs and are thought to be signposts of their early phases of formation. Our discovery makes IRAS 16547−4247 the most luminous ($\sim 6.2 \times 10^4\ L_\odot$) YSO from which a thermal jet emanates, suggesting that the mechanism that produces jets in low-mass YSOs also operates in high-mass YSOs.

2. OBSERVATIONS

The observations were made using ATCA in Australia and the 15 m Swedish–ESO Submillimetre Telescope (SEST)[2] located on La Silla, Chile.

[1] The Australia Telescope Compact Array is funded by the Commonwealth of Australia for operation as a National Facility managed by CSIRO.

[2] The Swedish-ESO Submillimetre Telescope (SEST) is operated jointly by the European Southern Observatory (ESO) and the Swedish Science Research Council (NFR).

2.1. *ATCA*

The ATCA radio continuum observations were made in 2000 May using the 6D configuration, which utilizes all six antennae and covers east-west baselines from 77 m to 5.9 km. Observations were made at four frequencies: 1.384, 2.496, 4.800, and 8.640 GHz, each with a bandwidth of 128 MHz. The phase center of the array was $\alpha = 16^{\rm h}58^{\rm m}16^{\rm s}.849$ and $\delta = -42^\circ 51' 37''.23$ (J2000.0). The total integration time at each frequency was about 60 minutes, obtained from 6 minute scans taken over a wide range of hour angles to provide good (u, v) plane coverage. The calibrator PKS 1612−52 was observed before and after every on-source scan in order to correct the amplitude and phase of the interferometer data for atmospheric and instrumental effects. Calibration of the bandpass was achieved from observations of 1740−517. The flux density was calibrated by observing PKS 1934−638 (3C 84) for which values of 14.94, 11.14, 5.83, and 2.84 Jy at 1.4, 2.5, 4.8, and 8.6 GHz were adopted. Standard calibration and data reduction were performed using MIRIAD (Sault, Teuben, & Wright 1995). Maps were made by Fourier transformation of the uniformly weighted interferometer data using the AIPS task MX. The noise levels achieved in the images are 0.38, 0.21, 0.096, and 0.070 mJy beam^{-1} and the synthesized (FWHM) beams $10''.23 \times 5''.71$, $5''.97 \times 3''.27$, $2''.81 \times 1''.83$, and $1''.62 \times 1''.01$ at the frequencies of 1.4, 2.5, 4.8, and 8.6 GHz, respectively.

2.2. *SEST*

2.2.1. *Millimeter Continuum*

The 1.2 mm continuum observations were made in 2001 September and 2002 July using the 37 channel SEST Imaging Bolometer Array (SIMBA). The half-power beamwidth of a single element is $24''$, and the separation between elements on the sky is $44''$. We made the observations in the fast-mapping mode, using a scan speed of $80''$ s^{-1}. Our observing blocks consisted of 50 scan lines in azimuth of length $800''$ and separated in elevation by $8''$, giving a map size in elevation of $400''$. This block required $\sim$15 minutes of observing time. Four blocks were observed in the first epoch and one in the second epoch. The data were reduced according to a standard procedure using the software package MOPSI, which included baseline subtraction and rejection of correlated sky noise. Flux calibration was performed using a sky-opacity correction and a counts-to-flux conversion factor derived from maps of bright planets. The rms noise level in the final map is 45 mJy with a pixel binning of $8''$. Uncertainties in the pointing accuracy are estimated at $3''$.

2.2.2. *Molecular Lines*

The molecular line observations were carried out during 1999 June. We used the high-resolution acousto-optical spectrometers which provided a channel separation of 43 kHz and a total bandwidth of 43 MHz. We observed at the position of the *IRAS* source the emission in the CS($2 \rightarrow 1$), CS($5 \rightarrow 4$), CS($7 \rightarrow 6$), $C^{34}S(2 \rightarrow 1)$, SiO($2 \rightarrow 1$), SO($6_5 \rightarrow 5_4$), $HCO^+(1 \rightarrow 0)$, $HCO^+(3 \rightarrow 2)$, $H^{13}CO^+(1 \rightarrow 0)$, $C^{18}O(2 \rightarrow 1)$, and $H_2S(2_{20} \rightarrow 2_{11})$ lines with integration times on source ranging from 3 to 6 minutes. System temperatures were typically $\sim$220 K at 3 mm, $\sim$350 K at 1 mm, and $\sim$700 K at 0.8 mm. In

addition, we mapped, with angular spacings of 30″, the $CS(2 \rightarrow 1)$, $CS(5 \rightarrow 4)$, $SiO(2 \rightarrow 1)$, and $SO(6_5 \rightarrow 5_4)$ emission across regions of 2′ centered on the *IRAS* position.

3. RESULTS

3.1. *Radio Continuum Emission*

Figure 1 shows maps of the radio continuum emission from IRAS 16547−4247 at the frequencies of 1.4, 2.5, 4.8, and 8.6 GHz. These maps show that the radio emission arises from three components in an almost linear structure along a direction with a P.A. of 161°. The outer components are symmetrically located in opposite directions from the central source, with peak positions separated by an angular distance of ∼20″ (0.28 pc at the distance of 2.9 kpc). The positions and flux densities of the three components are given in Table 1. Radio continuum observations toward IRAS 16547−4247 were previously made by Walsh et al. (1998), who reported that the central source has a flux density at 8.6 GHz of 5 mJy and is unresolved with a beam of 1.″5, in good agreement with our results.

Whereas at 1.4 GHz the three radio sources are blended and appear as a single elongated object, at 2.5 GHz, they appear as distinct structures. The map at 4.8 GHz shows that the morphology of the northwest lobe consists of a compact knot with a tail of more diffuse emission extending to the south. A Gaussian fit to the observed brightness distribution at 4.8 GHz gives deconvolved major and minor axes of 3.″7 and 0.″63 at P.A. 167°. The morphology of the southeast lobe is, on the other hand, unresolved at 4.8 and 8.6 GHz. The central bright object is unresolved at all frequencies. In the 8.6 GHz map, we also detected a compact source located about 4″ southeast of the bright central source.

Figure 2 shows the spectra of the integrated radio continuum emission from the three components. The observed spectra can be fitted by power laws of the form $S_\nu \propto \nu^\alpha$, where S_ν is the flux density at the frequency ν, and α is referred to as the spectral index. We find that the spectral index of the emission from the central object is positive, $\alpha = 0.49 \pm 0.12$, whereas those of the north and south lobes are negative, with values of -0.61 ± 0.26 and -0.33 ± 0.04, respectively.

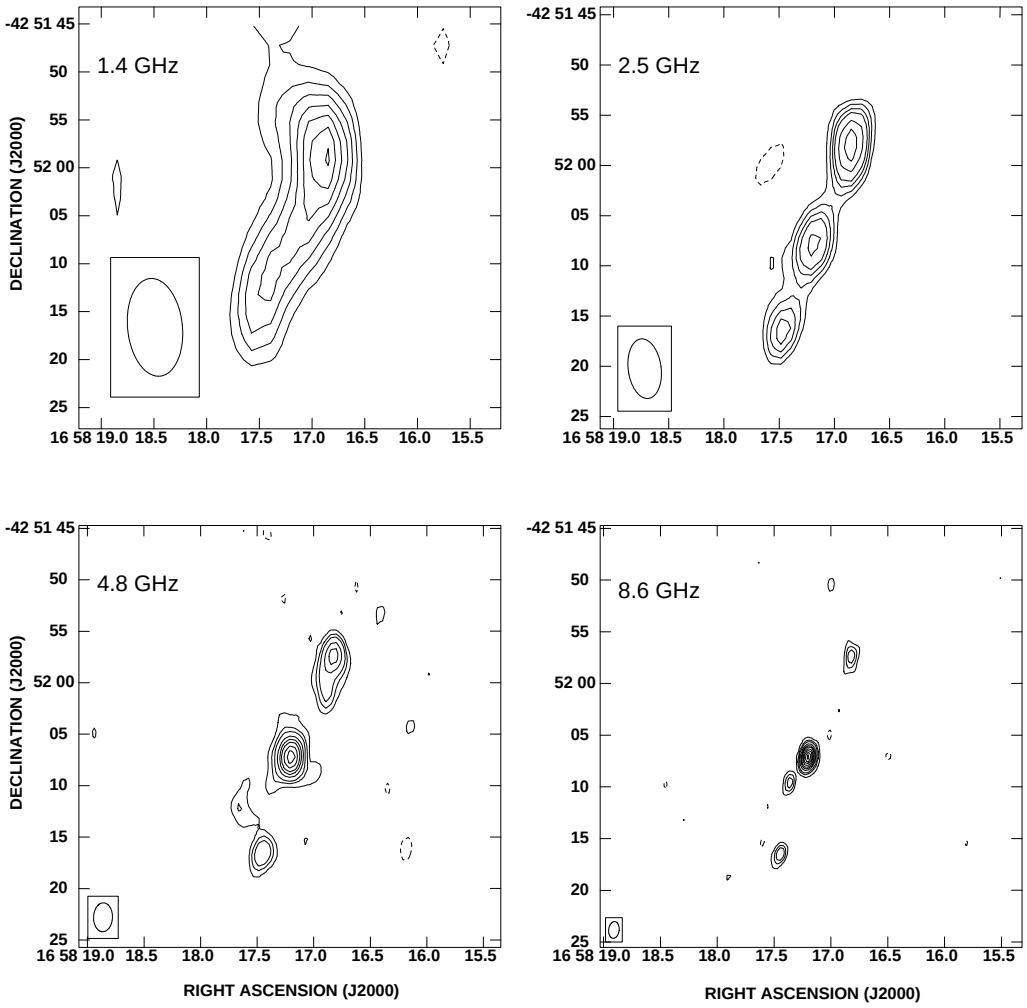

FIG. 1.—ATCA maps of the radio continuum emission from IRAS 16547−4247. Beams are shown in the lower left corner of each panel. *Top left*: 1.4 GHz map. Contour levels are −2, 2, 3, 4, 5, 6, 7, and 8 times 0.5 mJy beam^{-1} (1 σ = 0.38 mJy beam^{-1}). *Top right*: 2.5 GHz map. Contour levels are −2, 2, 3, 4, 5, 7, 9, and 11 times 0.35 mJy beam^{-1} (1 σ = 0.21 mJy beam^{-1}). *Bottom left*: 4.8 GHz map. Contour levels are −1, 1, 2, 3, 5, 7, 9, 12, and 15 times 0.30 mJy beam^{-1} (1 σ = 0.096 mJy beam^{-1}). *Bottom right*: 8.6 GHz map. Contour levels are −1, 1, 2, 3, 5, 7, 9, 12, 15, and 18 times 0.30 mJy beam^{-1} (1 σ = 0.070 mJy beam^{-1}).

TABLE 1
OBSERVED PARAMETERS OF RADIO SOURCES

Source	Peak Position (J2000)		Flux Density (mJy)			
	α	δ	1.4 GHz	2.5 GHz	4.8 GHz	8.6 GHz
North lobe	16 58 16.821	−42 51 57.35	4.9 ± 0.5	3.8 ± 0.2	3.9 ± 0.3	1.4 ± 0.2
Central	16 58 17.202	−42 52 07.13	2.7 ± 0.4	3.1 ± 0.4	5.9 ± 0.2	6.0 ± 0.1
Central-southeast	16 58 17.362	−42 52 09.59	...	...	...	0.9 ± 0.1
South lobe	16 58 17.446	−42 52 16.48	2.1 ± 0.4	1.8 ± 0.2	1.5 ± 0.1	1.1 ± 0.1

NOTE.—Units of right ascension are hours, minutes, and seconds, and units of declination are degrees, arcminutes, and arcseconds.

3.2. *Millimeter Continuum Emission*

Figure 3 shows a map of the 1.2 mm continuum emission observed with SEST, revealing the presence of a strong dust continuum source. The 1.2 mm emission has a peak position at $\alpha = 16^h58^m17^s.24$, $\delta = -42°52'3''.8$ (J2000.0), a total flux density of 16.4 ± 0.5 Jy, and a peak flux density of 7.3 Jy beam^{-1}. The morphology of the emission is slightly elongated in the north-south direction, with deconvolved major and minor axes of 33″ and 25″ and a P.A. of 3°.

3.3. *Molecular Line Emission*

The molecular observations show that IRAS 16547−4247 is associated with a dense and massive molecular core. Figure 4 presents a map of the CS(5 → 4) emission showing that the spatial distribution of the dense molecular gas is roughly circular with a deconvolved angular size of 27″ (FWHM). This implies a diameter of 0.38 pc at a distance of 2.9 kpc. From the ratio of the velocity integrated emission in the CS(2 → 1) and $C^{34}S(2 \rightarrow 1)$ lines, assuming a $[CS/C^{34}S]$ abundance ratio of 22.5, we determined an optical depth in CS(2 → 1) through the center of the core of ∼4.7. Assuming an excitation temperature of 30 K and that the energy levels are populated according to local thermodynamic equilibrium, this implies a total CS column density of 6.2×10^{15} cm^{-2}. Assuming a path length equal to the observed diameter yields a CS density of 5.2×10^{-3} cm^{-3}. Furthermore, assuming a $[CS/H_2]$ abundance ratio of 1×10^{-8} (cf. van der Tak et al. 2000), we find that the molecular hydrogen density and the mass of molecular gas are 5.2×10^5 cm^{-3} and 9.0×10^2 $M_\odot$, respectively.

Figure 5 shows the spectra observed toward the peak position of IRAS 16547−4247. The CS(2 → 1), $HCO^+(1 \rightarrow 0)$ and $HCO^+(3 \rightarrow 2)$ spectra show double-peaked line profiles, with a bright blueshifted peak at the velocity of -32.1 ± 0.3 km s^{-1} and a weaker redshifted peak at the velocity of -26.2 ± 1.0 km s^{-1}. In contrast, the

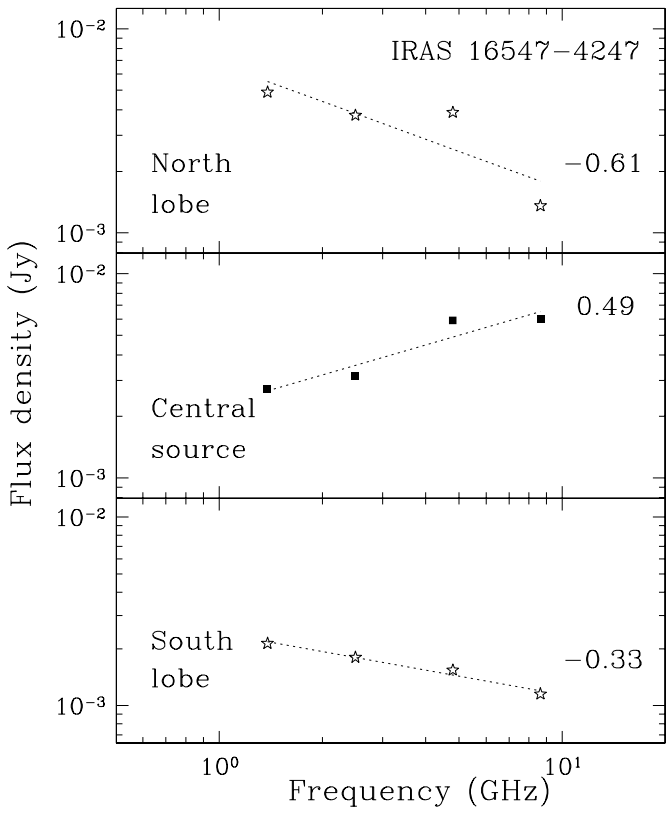

FIG. 2.—Radio continuum flux density vs. frequency for the three radio components toward IRAS 16547−4247. *Dotted lines*: Minimum least-squares power-law fits to the observed spectra. Shown is the fitted power-law index. *Top*: North lobe. *Middle*: Central object. *Bottom*: South lobe.

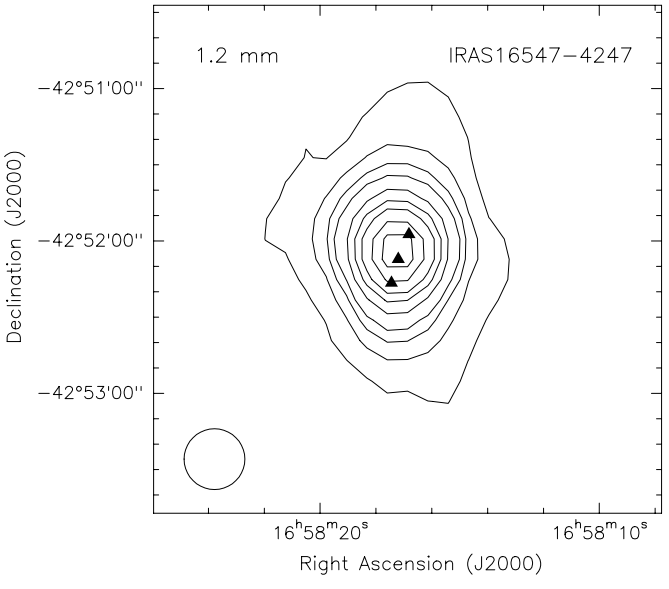

FIG. 3.—Map of the 1.2 mm continuum emission from IRAS 16547−4247 observed with SEST. The angular resolution is 24″ (*lower left corner*: FWHM beam). Contour levels are −0.4, 0.4, 0.8, 1.2, 1.6, 2.4, 3.2, 4.0, 5.2, and 6.4 Jy beam^{-1}. *Triangles*: Peak positions of the three radio components.

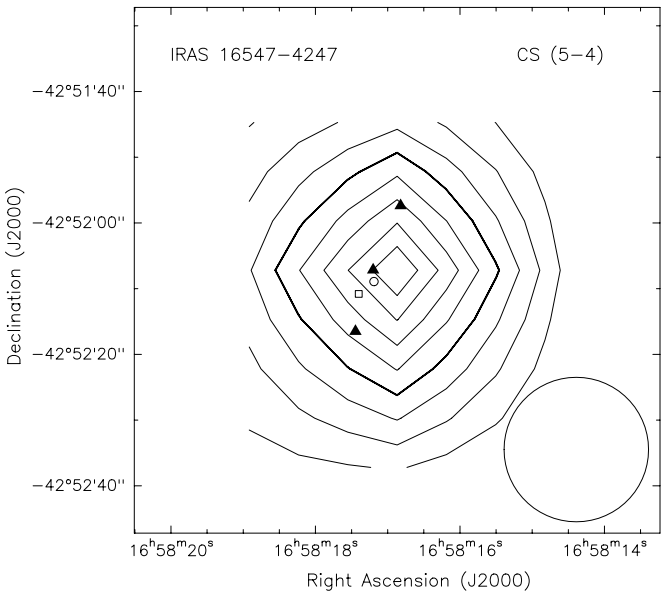

FIG. 4.—Map of the CS($5 \rightarrow 4$) line emission from IRAS 16547−4247 observed with SEST. The angular resolution is 22″ (*lower right corner*: FWHM beam). Contour levels are 20%, 30%, 40%, 50%, 60%, 70%, 80%, and 90% of the peak velocity integrated antenna temperature of 19.4 K km s^{-1}. *Triangles*: Peak positions of the three radio components. *Circle, square*: Position of the OH and H_2O masers, respectively.

profiles of the $C^{34}S(2 \rightarrow 1)$ and $H^{13}CO^+(1 \rightarrow 0)$ lines show an approximately symmetric single component with a peak line center velocity of −30.5 km s^{-1}. These spectroscopic signatures suggest that the bulk of the molecular gas toward IRAS 16547−4247 is undergoing large-scale inward motions. Infalling motions traced by optically thick molecular lines are expected to produce line profiles showing blue asymmetry, whereas optically thin lines are expected to exhibit symmetrical profiles (Mardones et al. 1997). In most species, the spectra show the presence of strong wing emission indicative of outflow activity. The line wing emission extends typically up to radial velocities of −19 and 16 km s^{-1} relative to the ambient cloud LSR velocity of -30.0 ± 0.3 km s^{-1}, determined from an average of several lines. Molecular outflows associated with high-mass YSOs are more energetic and tend to have larger opening angles than those associated with low-mass YSOs. This suggests that molecular outflows in high-mass YSOs are shaped by a wide-angle wind component. The angular resolution of our observations is too coarse to reveal the spatial distribution of the wing emission.

4. DISCUSSION

4.1. *The Host Environment*

Figure 6 shows the spectral energy distribution (SED) of IRAS 16547−4247 from 12 μm to 1.2 mm, the range in which the emission is due mainly to thermal dust emission. The total far-infrared luminosity of IRAS 16547−4247 computed using the *IRAS* fluxes (see Casoli et al. 1986) is $\sim 6.2 \times 10^4\ L_\odot$ (assuming a distance of 2.9 kpc; L. Bronfman 2002, private communication). We fitted the SED with modified blackbody functions of the form $B_\nu(T_d)[1 - \exp(-\tau_\nu)]\Omega_s$, where τ_ν is the dust optical depth, $B_\nu(T_d)$ is the Planck function at the dust temperature T_d, and Ω_s is the solid angle subtended by the dust-emitting region. The opacity was assumed to vary with frequency as ν^β, i.e., $\tau_\nu = (\nu/\nu_o)^\beta$, where ν_o is the frequency at which the optical depth is unity. Due to the limited number of spectral points, we have set the value of β equal to 2.0, consistent with tabulated opacities (Ossenkopf & Henning 1994) and derived values for high-mass star-forming regions (Molinari et al. 2000). A single-temperature model produced poor fits, underestimating the emission observed at wavelengths shorter than 25 μm, and therefore, we used a model with two temperature components. The luminosity obtained from integrating under the fitted curve in Figure 6 is similar to the *IRAS* luminosity.

From the fit (*long-dashed line*), we derive that the colder dust component (*short-dashed line*) has a temperature of 30 K, an angular size (assuming a Gaussian flux distribution) of 28″ (FWHM), and a wavelength at which the opacity is unity of $\sim$190 μm. The temperature of the hot dust component is 100 K. The thermal dust emission at 1.2 mm is therefore optically thin ($\tau_{1.2\,\mathrm{mm}} \sim 2 \times 10^{-2}$), and thus, the observed flux density at 1.2 mm allows us to obtain an additional mass estimate of the dense core. Following Chini, Krugel, & Wargau (1987), adopting a dust opacity at 1.2 mm of 1 cm^2 g^{-1} appropriate for dense and cold protostellar cores (Ossenkopf & Henning 1994), a dust-to-gas mass ratio of 0.01, and using the fitted dust temperature and the observed flux density, we derive a mass of $1.3 \times 10^3\ M_\odot$.

4.2. *The Nature of the Triple Radio Source*

The radio continuum observations toward IRAS 16547−4247 indicate the presence of a triple system consisting of a bright and compact central source and two lobes, extending up to 0.14 pc from the central object, aligned in an almost linear structure. The central component is coincident, within the errors, with the position of the *IRAS* source. It is also associated with OH and H_2O maser spots (Forster & Caswell 1989; Caswell 1998), with velocities close to the radial velocity of the ambient cloud. Further, it lies at the peak of the continuum dust emission mapped with SIMBA. These circumstances strongly suggest that the triple radio system is associated with the galactic massive star-forming region and is not of extragalactic origin. The probability of finding an extragalactic source at 5 GHz with a flux density above 1 mJy in a region of $1' \times 1'$ is 7×10^{-3} (Fomalont et al. 1991).

The radio continuum spectra of the central object is well fitted by a power law with a spectral index of 0.49 ± 0.12 (Fig. 2, *middle panel, dotted line*). This suggests that the emission is free-free emission arising from a thermal jet. Theoretical calculations show that for a collimated wind of constant temperature, velocity, and ionization fraction, the flux density depends on frequency as $S_\nu \propto \nu^{1.3-0.7/\epsilon}$, where ϵ is the power-law index that describes the dependence of the jet half-width with the distance to the jet origin (Reynolds 1986). The observed spectral index implies $\epsilon \sim 0.9$, a value close to that of a biconical jet. The theoretical calculations also predict that the angular size of the source depends on frequency as $\theta_{\mathrm{maj}} \propto \nu^{-0.7/\epsilon}$. However, the coarse angular resolution of our observations does not allow us to investigate this dependence. Clearly, observations with higher angular resolution are needed to resolve the jet. Assuming that the central source is a biconical jet, then equation (19) of Reynolds (1986) yields, for a distance of 2.9 kpc and an

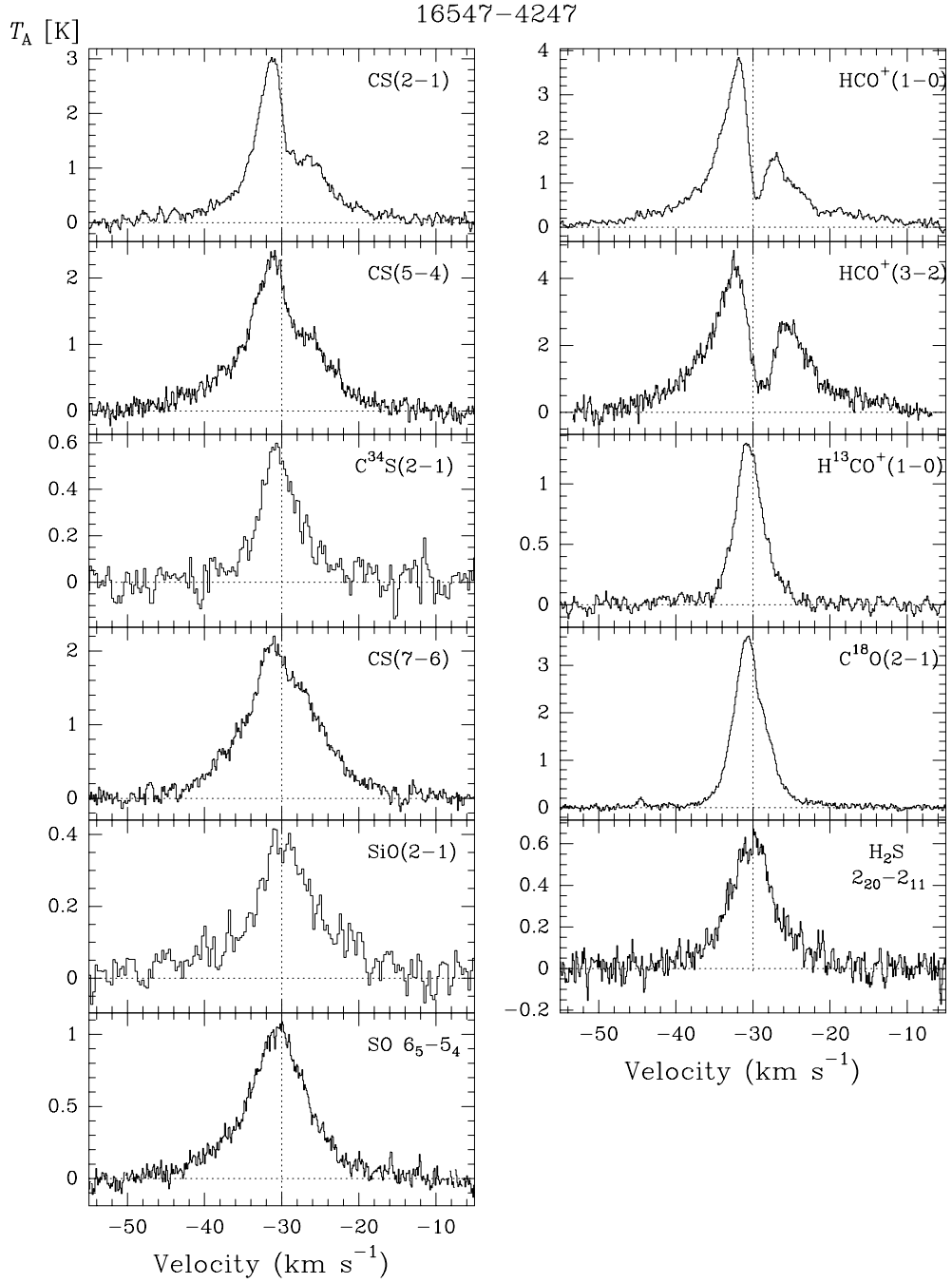

FIG. 5.—Spectra of the emission in several molecular lines observed toward the peak position of the IRAS 16547−4247 massive core. Transitions are given in the upper right corner of the spectra. *Vertical dotted line*: Systemic velocity of the ambient gas of −30.0 km s^{-1}.

observed flux density at 8.6 GHz of 6 mJy, the following constraint on the jet physical parameters:

$$\left(\frac{\dot{M}_w}{10^{-6}\ M_\odot\ \mathrm{yr}^{-1}}\right) = 7.7\left(\frac{v_w}{10^3\ \mathrm{km\ s}^{-1}}\right) \times \left(\frac{\theta}{0.4}\right)^{3/4}\left(\frac{\sin i}{\sin 45^\circ}\right)^{-1/4},$$

where $\dot{M}_w$ is the mass-loss rate, v_w the wind velocity, θ the opening angle at the base of the jet, and i the inclination angle with respect to the line of sight. None of these parameters are known. Assuming that the normalization values of v_w and θ, typical of jets associated with luminous objects, are appropriate for the IRAS 16547−4247 jet, then the constraint equation implies that its mass-loss rate is $\sim 8 \times 10^{-6}$ $M_\odot$ yr^{-1}. Shock-induced ionization has been proposed as the mechanism best able to explain the radio emission of most jets associated with low-luminosity energy sources (Anglada et al. 1998). In the case of IRAS 16547−4247, the driving source is thought to be highly luminous, and hence, stellar UV photons may be the source of ionization. In § 4.3, we argue, however, that UV photons are not able to reach far from the stellar surface, and thus, they are not available for the ionization of the neutral jet. Thus, we suggest that the source of ionization of the IRAS 16547−4247 jet is UV

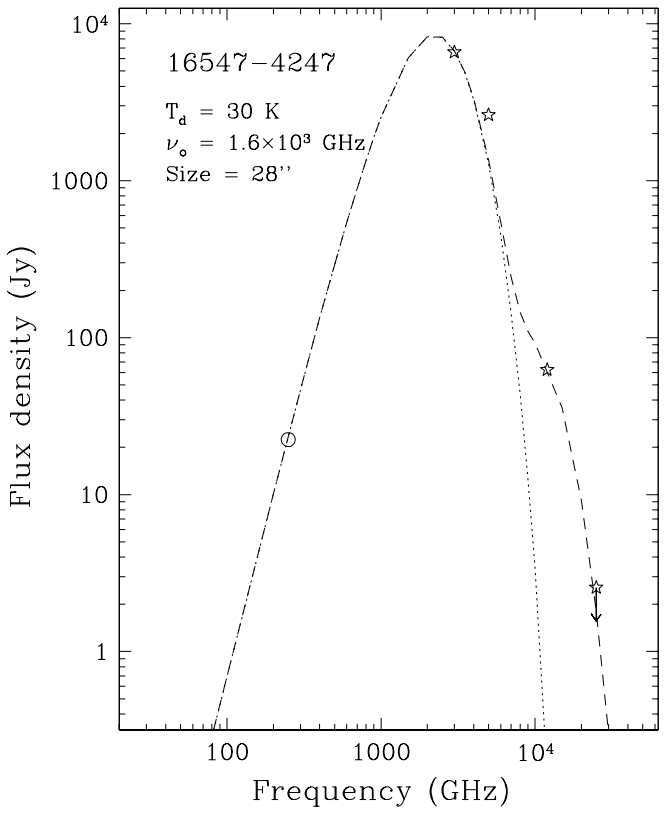

FIG. 6.—Spectral energy distribution of IRAS 16547−4247. *Stars*: IRAS fluxes. The 12 μm value is an upper limit. *Circle*: SIMBA flux. *Long-dashed curve*: Fit to the spectrum using two modified blackbody functions of the form $B_\nu(T_d)\{1 - \exp[-(\nu/\nu_o)^\beta]\}$, with different temperatures. *Short-dashed line*: Fit for the colder temperature component (*upper left*: fit parameters).

photons produced when a neutral wind shocks against surrounding high-density material (Curiel, Cantó, & Rodríguez 1987).

The spectral indices of the radio emission from the lobes differ significantly from the value of −0.1 expected for optically thin free-free emission and suggest that the emission is nonthermal. Rodríguez et al. (1993) have shown that sharply negative spectral indices cannot occur for free-free emission, regardless of the electron density and temperature distribution. Radio sources with negative spectral indices within star-forming regions already have been found by Rodríguez et al. (1989), Yusef-Zadeh et al. (1990), Martí, Rodríguez, & Reipurth (1993), Curiel et al. (1993), Reid et al. (1995), and Garay et al. (1996). We suggest that the radio emission from the lobes arises in shocks resulting from the interaction of a collimated stellar wind with the surrounding medium. In shock waves moving through a magnetized medium, a small fraction of the electrons are accelerated to relativistic velocities, giving rise to nonthermal synchrotron emission, while most of the electrons produce thermal free-free emission (Crusius-Wätzel 1990; Henriksen, Ptuskin, & Mirabel 1991). The production of relativistic electrons is understood in terms of a diffusive shock-wave acceleration mechanism in which the electrons are accelerated by traversing the shock many times due to scattering off magnetohydrodynamic irregularities (cf. Crusius-Wätzel 1990). The theory of this mechanism has been reviewed by Blandford & Eichler (1987). For a strong shock, a synchrotron spectral index close to −0.5 is expected.

A triple radio source with the above characteristics, exhibiting a central object and two lobes and associated with a star-forming region, has been found previously in the Serpens region (Rodríguez et al. 1980; Snell & Bally 1986). The emission from the lobes also shows negative spectral indices (Curiel et al. 1993). Monitoring observations show that the outer components are moving away from the central source with velocities of ∼300 km s^{-1} (Rodríguez et al. 1989). The kinematic age of the expansion is ∼50 yr. In IRAS 16547−4247, the lobes are at a projected distance of ∼0.14 pc of the central source. Assuming that the collimated wind has the velocity of ∼10^3 km s^{-1} typical of jets associated with luminous objects (HH 80-81: Martí, Rodríguez, & Reipurth 1995; Cepheus A HW2: Rodríguez et al. 2001), we estimate that this radio system has a dynamical age of about 140 yr. There is, however, a notable difference between the IRAS 16547−4247 and Serpens systems. The energy source of the Serpens radio jet is a young, low-luminosity star ($L_b \sim 300\ L_\odot$; Harvey, Wilking, & Joy 1984), whereas that of IRAS 16547−4247 is a young, high-luminosity star ($L_b \sim 6.2 \times 10^4\ L_\odot$). Finally, we note that there is a slight misalignment between the lobes and the central source of the IRAS 16547−4247 system that could be explained in terms of a model of a jet ejected from a source with an orbital motion (Masciadri & Raga 2002).

4.3. *Evolutionary Stage*

The high luminosity of IRAS 16547−4247 suggests that the massive core hosts a young massive protostar inside. If the luminosity is produced by a ZAMS star, it would be an O8 star, which emits a rate of ionizing photons of 2.2×10^{48} s^{-1} (Panagia 1973). If embedded in a constant density medium, this star is expected to generate an H II region with a flux density of ∼2.7 Jy at optically thin radio frequencies, far in excess of the observed value of ∼6 mJy. We suggest that the weak radio emission from the central source is a consequence of the fact that IRAS 16547−4247 is still undergoing an intense accretion phase, with the central object still being in the pre–main-sequence phase. The high mass accretion rate of the infalling material forbids the development of a sizeable H II region (Yorke 1984; Walmsley 1995), and the free-free emission from the ionized material is considerably lowered at centimeter wavelengths.

This hypothesis is supported by the characteristics of the line profiles observed toward IRAS 16547−4247, which suggest that the molecular gas is undergoing large-scale infalling motions. From the spectra of the optically thick $HCO^+(1 \rightarrow 0)$ line, we measure a velocity difference between the red and blue peaks of 4.9 km s^{-1} and brightness temperature of the blue peak, red peak, and dip of 5.1, 2.2, and 0.87 K, respectively. From the spectra of the optically thin $H^{13}CO^+(1 \rightarrow 0)$ line, we measure a FWHM line width of 4.4 km s^{-1}. From these values, using the simple model of contracting clouds of Myers et al. (1996), we derive a characteristic inward speed of 0.75 km s^{-1}. We note that this value is considerably smaller than the free-fall velocity expected for a cloud with a total mass of $\sim 1 \times 10^3\ M_\odot$ at its outer envelope radius of 0.27 pc, suggesting that the collapse is not dynamical. Using the derived values of the infall speed, molecular density, and core size, we obtain a mass infall rate, $\dot{M}_{\rm in}$, of $\sim 1 \times 10^{-2}\ M_\odot$ yr^{-1}, large enough to prevent the development of a UC H II region. The high value of

the mass infall rate raises the question as to which is the fraction of the total luminosity due to accretion. The accretion luminosity, $L_{\rm acc}$, is

$$L_{\rm acc} = f \frac{G\ \dot{M}_{\rm in}\ M_p}{R_p}\ ,$$

where f is the fraction of the large-scale mass infall rate that goes into accretion onto the protostar, M_p is the mass of the protostar, and R_p the radius where the shock occurs. None of these three parameters are known for IRAS 16547−4247. Assuming $M_p \sim 20\ M_\odot$, $R_p \sim 4 \times 10^{12}$ cm (Norberg & Maeder 2000), and $f \sim 0.1$, we obtain $L_{\rm acc} \sim 1 \times 10^4\ L_\odot$, about 20% of the total luminosity. We emphasize that this value of the accretion luminosity corresponds only to a rough estimate, particularly because the value of f is highly uncertain.

The early evolutionary stage of this region is also sustained by the presence of OH masers (Caswell & Haynes 1983; Caswell 1998) and H_2O masers (Batchelor et al. 1980; Forster & Caswell 1989), which are thought to be signposts of young regions of massive star formation (see Garay & Lizano 1999 and references therein). No methanol masers were detected toward this source in the survey by Walsh et al. (1998). The OH maser center of activity is associated with the central bright radio source, its position being displaced 1″.8 south of the peak position of the radio object. On the other hand, the H_2O maser center of activity is located about 4″ southeast of the central bright source, being closer to the weak central source detected at 8.6 GHz. H_2O masers are known to exhibit a dichotomy in their role as tracers: they appear to be related morphologically and kinematically either with thermal jets (Chernin 1995; Claussen et al. 1998) or with disks (Torrelles et al. 1998) around YSOs. The type of role played by the H_2O masers in this case is uncertain, mainly because of the lack of knowledge about the nature of the weak radio source. Whether this object contains an energy source of its own or is associated with the wind activity from the central jet, due for instance to precession, is difficult to assess.

5. SUMMARY

We made radio continuum observations at 1.4, 2.5, 4.8, and 8.6 GHz using ATCA and 1.2 mm continuum and molecular-line observations using SEST toward IRAS 16547−4247, a luminous object ($L \sim 6 \times 10^4\ L_\odot$) thought to be a massive star-forming region in an early stage of evolution. The main results and conclusions are summarized as follows:

1. The radio continuum observations show the presence of a triple radio source consisting of a compact central object and two outer lobes located in an almost linear structure with a P.A. of 161°. The lobes are separated by about 20″ and symmetrically located from the central source. The emission from the central object has a spectral index of 0.49, consistent with free-free emission from a thermal jet. From the observed flux density, we estimated a mass-loss rate of $\sim 8 \times 10^{-6}\ M_\odot\ {\rm yr}^{-1}$. The radio emission from the lobes has spectral indices of −0.61 and −0.33, characteristic of nonthermal emission. We suggest that the radio emission from the central object originates in a highly collimated ionized wind, whereas the emission from the lobes results from the interaction of the collimated wind with the surrounding medium.

2. The 1.2 mm continuum observations show strong dust emission arising from a region with major and minor axes of 33″ and 25″, respectively. The observed flux density at 1.2 mm of 16.4 ± 0.7 Jy, implies a mass of $1.3 \times 10^3\ M_\odot$.

3. The line observations indicate that IRAS 16547−4247 is associated with a molecular core with a diameter of 0.38 pc, a molecular hydrogen density of 5.2×10^5 cm^{-3}, and a mass of $9.0 \times 10^2\ M_\odot$. The line profiles indicate that the bulk of the molecular gas is undergoing large-scale inward motions, with a characteristic infall speed of 0.75 km s^{-1}, implying a mass infall rate of $\sim 1 \times 10^{-2}\ M_\odot\ {\rm yr}^{-1}$. They also show strong wing emission up to radial velocities of ±18 km s^{-1} relative to the ambient cloud velocity, indicating outflow activity. We suggest that this massive, dense core is in an early stage of collapse, accreting at high rates that prevent the formation of a detectable photoionized UC H II region.

4. We conclude that IRAS 16547−4247 hosts a jet powered by a massive star in the process of formation, with the outer radio lobes being a manifestation of the collimated mass-loss activity of the central object, corresponding to regions of shocked gas at the working surfaces of the jet. The remarkable similarity between the well-collimated triple source in IRAS 16547−4247 and those associated with low-luminosity YSOs (e.g., Serpens) suggests that high-mass YSOs pass through similar evolutionary phases.

K. B., G. G., and D. M. gratefully acknowledge support from the Chilean Centro de Astrofísica FONDAP 15010003. G. G. also acknowledges support from FONDECYT project 1010531.

REFERENCES

Anglada, G., Villuendas, E., Estalella, R., Beltrán, M. T., Rodríguez, L. F., Torrelles, J. M., & Curiel, S. 1998, AJ, 116, 2953
Bally, J., & Lada, C. J. 1983, ApJ, 265, 824
Batchelor, R. A., Caswell, J. L., Haynes, R. F., Wellington, K. J., Goss, W. M., & Knowles, S. H. 1980, Australian J. Phys., 33, 139
Beuther, H., Schilke, P., Sridharan, T. K., Menten, K. M., Walmsley, C. M., & Wyrowski, F. 2002, A&A, 383, 892
Blandford, R., & Eichler, D. 1987, Phys. Rep., 154, 1
Bonnell, I. A., Bate, M. R., & Zinnecker, H. 1998, MNRAS, 298, 93
Bronfman, L., Nyman, L. A., & May, J. 1996, A&AS, 115, 81
Casoli, F., Dupraz, C., Gerin, M., Combes, F., & Boulanger, F. 1986, A&A, 169, 281
Caswell, J. L. 1998, MNRAS, 297, 215
Caswell, J. L., & Haynes, R. F. 1983, Australian J. Phys., 36, 361
Cesaroni, R., Felli, M., Testi, L., Walmsley, C. M., & Olmi, L. 1997, A&A, 325, 725
Cesaroni, R., Walmsley, C. M., Kömpe, C., & Churchwell, E. 1991, A&A, 252, 278
Chernin, L. M. 1995, ApJ, 440, L97
Chini, R., Krügel, E., & Wargau, W. 1987, A&A, 181, 378
Churchwell, E. 2000, Unsolved Problems in Stellar Evolution, ed. M. Livio (Cambridge: Cambridge Univ. Press)
Churchwell, E., Walmsley, C. M., & Cesaroni, R. 1990, A&AS, 83, 119
Claussen, M. J., Marvel, K. B., Wootten, A., & Wilking, B. A. 1998, ApJ, 507, L79
Crusius-Wätzel, A. R. 1990, ApJ, 361, L49
Curiel, S., Cantó, J., & Rodríguez, L. F. 1987, Rev. Mexicana Astron. Astrofis., 14, 595
Curiel, S., Rodríguez, L. F., Moran, J. M., & Cantó, J. 1993, ApJ, 415, 191
Devine, D., Bally, J., Reipurth, B., Shepherd, D., & Watson, A. 1999, AJ, 117, 2919
Evans, N. J., II. 1999, ARA&A, 37, 311
Fomalont, E. B., Windhorst, R. A., Kristian, J. A., & Kellerman, K. I. 1991, AJ, 102, 1258
Forster, J. R., & Caswell, J. L. 1989, A&A, 213, 339
Garay, G., & Lizano, S. 1999, PASP, 111, 1049
Garay, G., Ramírez, S., Rodríguez, L. F., Curiel, S., & Torrelles, J. M. 1996, ApJ, 459, 193

Harvey, P. M., Wilking, B. A., & Joy, M. 1984, ApJ, 278, 156
Henriksen, R. N., Ptuskin, V. S., & Mirabel, I. F. 1991, A&A, 248, 221
Kwan, J., & Scoville, N. 1976, ApJ, 210, 39
Lada, C. J. 1985, ARA&A, 23, 267
———. 1991, The Physics of Star Formation and Early Stellar Evolution, ed. C. J. Lada & N. D. Kylafis (Dordrecht: Kluwer), 329
Mardones, D. 1998, Ph.D. thesis, Harvard Univ.
Mardones, D., Myers, P. C., Tafalla, M., Wilner, D. J., Bachiller, R., & Garay, G. 1997, ApJ, 489, 719
Martí, J., Rodríguez, L. F., & Reipurth, B. 1993, ApJ, 416, 208
———. 1995, ApJ, 449, 184
Masciadri, E., & Raga, A. C. 2002, ApJ, 568, 733
McKee, C., & Tan, J. C. 2002, Nature, 416, 59
Molinari, S., Brand, J., Cesaroni, R., & Palla, F. 2000, A&A, 355, 617
Myers, P. C., Mardones, D., Tafalla, M., Williams, J. P., & Wilner, D. J. 1996, ApJ, 465, L133
Norberg, P., & Maeder, A. 2000, A&A, 359, 1025
Osorio, M., Lizano, S., & D'Alessio, P. 1999, ApJ, 525, 808
Ossenkopf, V., & Henning, Th. 1994, A&A, 291, 943
Panagia, N. 1973, AJ, 78, 929
Plume, R., Jaffe, D. T., & Evans, N. J., II. 1992, ApJS, 78, 505
Reynolds, S. P. 1986, ApJ, 304, 713
Reid, M. J., Argon, A. L., Masson, C. R., Menten, K. M., & Moran, J. M. 1995, ApJ, 443, 238
Rodríguez, L. F., Curiel, S., Moran, J. M., Mirabel, I. F., Roth, M., & Garay, G. 1989, ApJ, 346, L85
Rodríguez, L. F., Garay, G., Curiel, S., Ramírez, S., Torrelles, J. M., Gómez, Y., & Velazquez, A. 1994, ApJ, 430, L65
Rodríguez, L. F., Ho, P. T. P., & Moran, J. M. 1980, ApJ, 240, L149
Rodríguez, L. F., Martí, J., Cantó, J., Moran, J. M., & Curiel, S. 1993, Rev. Mexicana Astron. Astrofis., 25, 23
Rodríguez, L. F., Moran, J. M., Gottlieb, E. W., & Ho, P. T. P. 1980, ApJ, 235, 845
Rodríguez, L. F., Torrelles, J. M., Anglada, G., & Martí, J. 2001, Rev. Mexicana Astron. Astrofis., 37, 95
Sault, R. J., Teuben, P. J., & Wright, M. C. H. 1995, in ASP Conf. Ser. 77, Astronomical Data Analysis Software and Systems IV, ed. R. A. Shaw, H. E. Payne, & J. J. E. Hayes (San Francisco: ASP), 433
Shepherd, D. S., & Churchwell, E. 1996, ApJ, 472, 225
Shepherd, D. S., Claussen, M. J., & Kurtz, S. E. 2001, Science, 292, 1513
Shepherd, D. S., Testi, L., & Stark, D. P. 2003, ApJ, 584, 882
Shepherd, D. S., Watson, A. M., Sargent, A. I., & Churchwell, E. 1998, ApJ, 507, 861
Shu, F. H., Adams, F. C., & Lizano, S. 1987, ARA&A, 25, 23
Shu, F. H., Najita, J., Galli, D., Ostriker, E., & Lizano, S. 1993, Protostars and Planets III, ed. E. H. Levy & J. I. Lunine (Tuscon: Univ. Arizona Press), 3
Snell, R. L., & Bally, J. 1986, ApJ, 303, 683
Stahler, S. W., Palla, F., & Ho, P. T. P. 2000, Protostars and Planets IV, ed. V. Mannings, A. P. Boss, & S. S. Russell (Tucson: Univ. Arizona Press), 327
Torrelles, J. M., Gómez, J. F., Rodríguez, L. F., Curiel, S., Anglada, G., & Ho, P. T. P. 1998, ApJ, 505, 756
van der Tak, F. F. S., van Dishoeck, E. F., Evans, N. J., II, & Blake, G. A. 2000, ApJ, 537, 283
Walmsley, C. M. 1995, Rev. Mexicana Astron. Astrofis. Ser. Conf. 1, 137
Walsh, A. J., Burton, M. G., Hyland, A. R., & Robinson, G. 1998, MNRAS, 301, 640
Yorke, H. W. 1984, Workshop on Star Formation, ed. R. D. Wolstencroft (Edinburgh: Royal Obs.), 63
Yusef-Zadeh, F., Cornwell, T. J., Reipurth, B., & Roth, M. 1990, ApJ, 348, L61
Zhang, Q., Hunter, T. R., Brand, J., Sridharan, T. K., Molinari, S., Kramer, M. A., & Cesaroni, R. 2001, ApJ, 552, L167